Ostwald Ripening in Thin Film Equations

K. B. Glasner

March 15, 2007

Abstract

Fourth order thin film equations can have late stage dynamics that arise in a fashion analogous to the classical Cahn Hilliard equation. Profound differences arise however, both because energetics give rise to near-equilibrium droplets and degenerate kinetics produce migration effects. We undertake here a systematic asymptotic analysis of a class of equations that describe partial wetting with a stable precursor film introduced by intermolecular interactions. The limit of small precursor film thickness is considered, leading to explicit expressions for the late stage dynamics of droplets. Our main finding is that exchange of mass between droplets characteristic of traditional Ostwald ripening is a subdominant effect over a wide range of kinetic exponents. Instead, droplets migrate in response to variations of the precursor film. Timescales for these processes are computed using an effective medium approximation to the reduced free boundary problem.

1 Introduction

Thin films of viscous fluids coating solid surfaces are known to produce complex dewetting instabilities [1, 2, 10, 17–19, 22]. These instabilities cause nearly-uniform fluid layers to break-up into arrays of large droplets connected by a remaining (very) thin film, which undergo an elaborate coarsening process characterized both by coalescence of droplets and exchange of fluid between droplets and the intervening film [5, 6, 8, 9].

The results we describe run parallel to other studies of dynamical coarsening processes, most notably phase separation phenomena described by the Cahn-Hilliard equation [3, 15]. At late times and small volume fractions, this equation describes the Ostwald ripening process [7, 11, 12, 20, 21]. Our purpose is to describe a similar limit for a class of thin film equations, and highlight the differences between our problem and classical Ostwald ripening.

This paper is a continuation of a body of work initiated by Glasner and Witelski [5, 6] on coarsening behavior of liquid droplets described by disjoining-pressure models. It was found there that the dewetting instability leads to the eventual development of droplets separated by a precursor film. The subsequent one-dimensional dynamics of these droplets was computed, involving both mass exchange between droplets and the precursor layer as well as motion of the droplets themselves. This results in a coarsening process characterized by dynamic scaling with a non-standard exponent. Rigorous bounds for dynamic scaling were subsequently obtained by Otto, Rump, and Slepcev [14]. In two dimensions, the interaction of droplets has been studied by Pismen and Pomeau [16]. Although not entirely dissimilar from the conclusions described here, their results are in both quantitative and qualitative disagreement with our calculations.

This work serves as a companion paper to the manuscript of Glasner, Otto, Rump and Slepcev [4]. Instead of a matched asymptotics approach, that work utilizes a variational principle (the Rayleigh-Onsager notion of least dissipation [13]) to explain and quantify droplet migration effects. Both papers obtain comparable results, although a careful interpretation is needed to show their equivalence. Some comparison is provided in section 5.

This paper considers a class of fourth order parabolic equations which have the structure

$$\tau(\epsilon)h_t = \nabla\cdot(h^q\nabla p), \quad p = \epsilon^{-1}U'\left(\frac{h}{\epsilon}\right) - \Delta h, \quad q > 0 \tag{1}$$

The physical domain is taken to be a two dimensional, bounded, simply connected open set Ω, where Neumann and no-flux boundary conditions are imposed (although few of our results depend crucially on these assumptions). The timescale $\tau(\epsilon)$ is chosen to capture the slow dynamics associated with migration and mass exchange (i.e. ripening) of droplets. It depends on the mobility exponent as

$$\tau(\epsilon) = \begin{cases} \epsilon^q & q \in (0,2) \\ \epsilon^2 \ln(\epsilon^{-1}) & q = 2 \\ \epsilon^2 & q \in (2,3) \\ \epsilon^2/\ln(\epsilon^{-1}) & q = 3 \\ \epsilon^{q-1} & q > 3 \end{cases} \tag{2}$$

Our interest is in the limit of small ϵ, which corresponds to both thin precursor films and long timescales. The following assumptions are placed on the potential U:

1. U is scaled so that it has a minimum at 1 and $U(\infty) - U(1) = 2$.

2. U' has a unique maximum at $H^* > 1$.

3. The potential decays as

$$U'(H) = \mathcal{O}(H^{-\alpha}), \quad H \to \infty \tag{3}$$

where

$$\alpha > \begin{cases} q+1 & q \in (0,2) \\ 3 & q \geq 2. \end{cases} \tag{4}$$

This will ensure that intermolecular interactions have a subdominant effect for macroscopic ($h \sim \mathcal{O}(1)$) films.

The structure of the paper is as follows. Section 2 describes the results of the lengthy calculation, whose details are given in sections 3 and 4. Section 5 goes on to propose an approximation procedure for the resulting free boundary problem, and timescales for the relevant dynamics are worked out. Section 6 gives example calculations and compares them to predictions of dynamic scaling.

2 Setup for matched asymptotics and a summary of results

There will be three regions in the matched asymptotic analysis:

- Region I: This region corresponds to droplets, and is composed of the union of disjoint disks $\{D_i\}$ which have the form $D = \{\mathbf{x} \Big| |\mathbf{x} - X| < R\}$ so that X is the droplet center and R is its radius. Unit normals to ∂D will be denoted $\mathbf{n}$, and we will also utilize the coordinate unit vectors $\hat{\mathbf{x}}, \hat{\mathbf{y}}$ etc. In this region, h and x will both scale like $\mathcal{O}(1)$. It will be convenient to use the moving polar coordinates $r = |\mathbf{x} - X(t)|, \theta = \arg(\mathbf{x} - X(t))$.

  To be more precise about R and X, we define (somewhat arbitrarily) the contact line at finite ϵ as the the set $\{\mathbf{x} | h(\mathbf{x}) = \epsilon H^*\}$ where H^* is the global maximum of U'. We suppose that for each droplet, this curve is nearly circular, and has the form $\mathbf{x} = X + R(\theta)\hat{\mathbf{r}}$. Properly speaking, R and X should also be expanded in ϵ, but to avoid excessive notation, these labels will simply denote the corresponding leading order solutions. In particular, we find R is independent of θ at leading order.

- Region II is a microscopic internal layer near the contact line where h and x scale like ϵ. The moving rescaled radial coordinate

$$z = \frac{R(t) - r}{\epsilon}. \tag{5}$$

will be employed. In light of the definition of R, the solution in this region must satisfy

$$h(z = 0) = h^*. \tag{6}$$

For reference, the Laplacian in z, θ coordinates expands as

$$\Delta h = \epsilon^{-2} h_{zz} - \epsilon^{-1} R^{-1} h_z - \left(z R^{-2} h_z + R^{-2} h_{\theta\theta} \right) + \mathcal{O}(\epsilon). \tag{7}$$

- Region III is the complement $\Omega / \cup D_i$ which contains the precursor film. In this region, h will scale like ϵ.

The overall strategy is to propose self-consistent asymptotic expansions in each region, and connect them via matching conditions. Less-standard matching conditions are derived when needed. Corrections to the leading order base solutions solve linear equations, and Fredholm-type solvability conditions will yield information about the dynamics.

The main goal is to determine the dynamic behavior of R and X, which will be shown to arise from a flux J which is determined by the elliptic problem

$$\Delta P = 0, \quad P|_{\partial D_i} = \frac{2}{R_i}, \quad J = -\nabla P. \tag{8}$$

solved in the exterior region $\Omega / \cup D_i$. Here P represents the first nontrivial correction to the pressure p. Equations (8) describe quasi-steady diffusion of material driven by a Gibbs-Thomson boundary condition. We find that, with respect to the timescale τ, the dynamics at leading order are

$$R_t = \begin{cases} -\frac{4}{3\pi R^2} \int_{\partial D} J \cdot \mathbf{n} \, ds & q < 2 \\ 0 & q \geq 2, \end{cases} \tag{9}$$

and

$$X_t = -M(R) \int_{\partial D} \mathbf{n} J \cdot \mathbf{n} \, ds, \tag{10}$$

where the mobility factor $M(R)$ is

$$M = \frac{1}{\pi}\begin{cases} R^{-2}\Psi_1(1)\Big/\int_0^1 \Psi_1(r)r^2dr & q<2 \\ R^{-2}\Big/\int_0^1 \Psi_1(r)r^2dr & q=2 \\ R^{q-4}\int_{-\infty}^{\infty} H_1^{1-q}-H_1^{-q}dz\Big/\int_0^1 \Psi_1(r)r^2dr & q\in(2,3) \\ R^{-1}\int_{-\infty}^{\infty} H_1^{-2}-H_1^{-3}dz & q=3 \\ R^{-1}\int_{-\infty}^{\infty} H_1^{1-q}-H_1^{-q}dz\Big/\int_{-\infty}^{\infty} H_1^{2-q}-H_1^{1-q}dz & q>3. \end{cases} \quad (11)$$

H_1 is the leading order solution for the microscopic contact line region II. The function Ψ_1 arises from the solvability argument and is specified as the solution of the rescaled boundary value problem (35)-(37).

3 Base solutions

This section summarizes the aspects of the analysis which is common to all mobility exponents $q > 0$. The rest is split into cases in the following section.

Region II. The solution is expanded as $h = \epsilon H_1 + \epsilon^2 H_2 + o(\epsilon^2)$. The leading order equation is

$$(H_1^q[-(H_1)_{zz} + U'(H_1)]_z)_z = 0 \quad (12)$$

Integrating twice and using the matching conditions $(H_1)_z \sim 0$ as $z \to -\infty$, we get

$$-(H_1)_{zz} + U'(H_0) = C. \quad (13)$$

The matching condition $(H_1)_{zz} \sim 0$ as $z \to +\infty$ means that $C = 0$ in light of (3). It follows that $H_1 \sim 1$ as $z \to -\infty$ and we can integrate again to obtain

$$\frac{1}{2}(H_1)_z^2 = U(H_1) - U(1), \quad (14)$$

from which the equilibrium contact angle is determined by

$$(H_1)_z = \sqrt{2[U(H_1) - U(1)]} \sim 1, \quad z \to +\infty. \quad (15)$$

Solving (14) gives the solution implicitly as

$$\int^{H_1} \frac{dH}{\sqrt{2[U(H) - U(1)]}} = z + C. \quad (16)$$

The constant of integration is determined uniquely by the condition (6).

The next order correction satisfies

$$(H_1^q[-(H_2)_{zz} - R^{-1}(H_1)_z + U''(H_1)H_2]_z)_z = 0 \tag{17}$$

Integrating and using the matching condition $(H_2)_{zzz} \to 0$ as $z \to \infty$ gives

$$[-(H_2)_{zz} - R^{-1}(H_1)_z + U''(H_1)H_2]_z = 0. \tag{18}$$

A further integration implies

$$-(H_2)_{zz} - R^{-1}(H_1)_z + U''(H_1)H_2 \equiv P = \text{constant} \tag{19}$$

This says that (total) leading order pressure is constant through region II, and we can use this to match between regions I and III. We remark that both H_1 and H_2 are independent of θ. Later in the calculation, this will provide symmetry that is needed to make certain integrals vanish.

Region I. Expanding $h = h_0(\mathbf{x}, t) + o(1)$ for now, we obtain

$$\nabla\cdot(h_0^q \nabla \Delta h_0) = 0, \quad \mathbf{x} \in D. \tag{20}$$

Provided h_0 is well behaved (bounded third derivatives), integration of (20) against Δh_0 gives

$$\int_D h_0^q |\nabla \Delta h_0|^2 dx = 0. \tag{21}$$

since $h_0 \to 0$ on the boundary of D, it follows Δh_0 is a constant. Using the matching conditions

$$h_0(R, \theta) = 0, \quad (h_0)_r(R, \theta) = -1. \tag{22}$$

gives the family of radially symmetric droplet solutions

$$h_0(\mathbf{x}; R(t), X(t)) = R(t) H\left(\frac{\mathbf{x} - X(t)}{R(t)}\right), \quad H(\eta) = \frac{1}{2}(1 - \eta^2). \tag{23}$$

Using (19,23) and the matching condition

$$(h_0)_{rr}(R, \theta) = \lim_{z\to\infty} (H_2)_{zz} \tag{24}$$

allows us to relate the pressure P and the droplet radius:

$$P = -\Delta h_0 = \frac{2}{R(t)}. \tag{25}$$

Region III. Here we expand $h = \epsilon h_1 + \epsilon^2 h_2 + o(\epsilon^2)$. Because of the scaling of $\tau(\epsilon)$, the leading order problem for all $q > 0$ is the elliptic equation

$$\nabla\cdot(h_1^q \nabla U'(h_1)) = 0. \tag{26}$$

Matching to region II implies $h_1 = 1$ on the boundary $\cup\partial D_i$, therefore $h_1 \equiv 1$. At order ϵ^2, the correction term satisfies the "quasisteady" problem

$$\Delta h_2 = 0. \tag{27}$$

This equation is solved together with boundary conditions that are derived by matching. Using (19) and (25) we find that

$$U''(1)h_2 = \frac{2}{R(t)}, \quad \mathbf{x} \in \partial D. \tag{28}$$

It is convenient introduce the flux

$$J = -h^q \nabla p = -\epsilon^q U''(1)\nabla h_2 + o(\epsilon^q). \tag{29}$$

so that at leading order

$$J_q = -\nabla P, \quad P \equiv U''(1)\nabla h_2 \tag{30}$$

is therefore determined by solving the boundary value problem (27), (28). To avoid excessive notation, we also use J_q to denote the flux of order $\mathcal{O}(\epsilon^q)$ in regions I and II.

4 Mobility-dependent expansions

4.1 Case $q \in (0, 2)$

The expansion of the equation in region II at order ϵ^q gives $0 = (J_q \cdot \hat{\mathbf{z}})_z$ which merely says that the z-component of J_q is constant through this layer. Thus the normal component of J_q to the boundary of D is that given by the solution in region III.

In region I, we expand $h = h_0(x,t) + \epsilon^q h_q + o(\epsilon^q)$, which means that leading order flux is $J_q = h_0^q \nabla\Delta h_q$. The first nontrivial correction to the equation in this region gives the linear problem

$$\mathcal{L}h_q = X_t \cdot \nabla h_0 - R_t \frac{\partial h_0}{\partial R}, \quad \mathcal{L} = (\nabla\cdot[h_0^q\nabla)\Delta \tag{31}$$

for $\mathbf{x} \in D$. The linear operator $\mathcal{L}$ (on a space endowed with suitable homogeneous boundary conditions) has the adjoint

$$\mathcal{L}^\dagger = \Delta\Big(\nabla\cdot[h_0^q\nabla\Big). \tag{32}$$

Nullspace of $\mathcal{L}^\dagger$. To invoke a Fredholm solvability argument, we need to characterize its nullspace by finding orthogonal functions whose span is the same as $\{(h_0)_x, (h_0)_y, (h_0)_R\}$. Observe that if ψ is in the nullspace, then

$$\nabla\cdot\Big[h_0^q\nabla\psi\Big] = \phi, \quad \Delta\phi = 0. \tag{33}$$

We shall be interested in the particular harmonic functions $\phi = 0, -x, -y$ which ultimately correspond to changes in droplet size and translation in each direction, respectively. Since $x = r\cos\theta, y = r\sin\theta$, we look for a solution of (33a) of the form $\psi = \Psi(r)\cos\theta$ or $\psi = \Psi(r)\sin\theta$. In either case we are led to the differential equation

$$r(rh_0^q\Psi')' - h_0^q\Psi = -r^3. \tag{34}$$

together with the boundary conditions

$$h_0^q\Psi'(R) = 0, \quad \Psi(0) = 0. \tag{35}$$

Several observations about (34)-(35) are in order. First, the solution is unique, since multiplying the homogeneous version of this linear equation by Ψ/r and integrating leads to

$$\int_0^R rh_0^q\Psi'^2 + \frac{h_0^q\Psi^2}{r}dr = 0. \tag{36}$$

There is also a natural scale invariance for this problem: If Ψ_1 solves

$$r(rH^q\Psi_1')' - H^q\Psi_1 = r^3, \quad \Psi_1(0) = 0, \quad H^q\Psi_1(1) = 0, \tag{37}$$

then

$$\Psi = R^{3-q}\Psi_1(r/R) \tag{38}$$

solves (34). Finally, the regularity of solutions of the ordinary differential equation (34) and the first boundary condition (35) allow us to ascertain the asymptotics at $r = R$. In particular, we have $h_0^q\Psi'(R) = \mathcal{O}(|r-R|)$ and therefore one computes for $r \to R$

$$\Psi \sim \begin{cases} \mathcal{O}(1) & q < 2 \\ R\ln|r-R| & q = 2 \\ \frac{R}{q-2}|r-R|^{2-q} & q > 2. \end{cases} \tag{39}$$

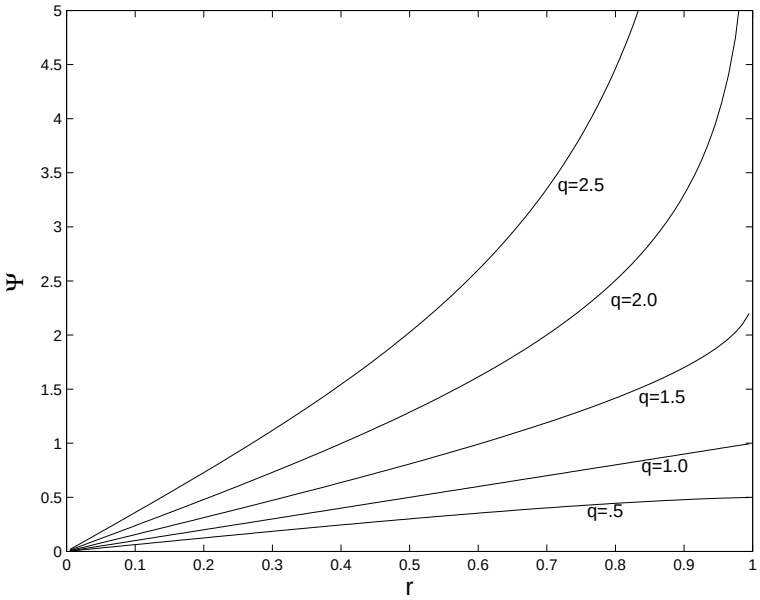

Figure 1: The function $\Psi(r)$ with $R = 1$, used in the solvability argument.

In particular, Ψ is bounded for $q < 2$ and integrable for $q < 3$. Since $r = R$ is a regular singular point of (34), the first boundary condition in (35) implies

$$h_0^q \Psi'(r) = \mathcal{O}(|r - R|), \quad r \to R. \tag{40}$$

In practice, solutions to (34) can be obtained numerically (see figure 1). To summarize, the desired functions for the solvability argument are

$$\psi_R = 1, \quad \psi_x = \Psi(r)\cos\theta, \quad \psi_y = \Psi(r)\sin\theta. \tag{41}$$

Solvability conditions. The inner product of ψ_R with (31) produces

$$R_t = -\frac{\int_{\partial D} h_0^q \nabla \Delta h_q \cdot \mathbf{n}\, ds}{\int_D \partial h_0/\partial R\, dx}. \tag{42}$$

Using the matching condition for flux,

$$R_t = -\frac{4}{3\pi R^2} \int_{\partial D} J_q \cdot \mathbf{n}\, ds. \tag{43}$$

This is just a reflection of conservation of the droplet mass $M = \pi R^3/4$ since

$$M_t = -\int_{\partial D} J_q \cdot \mathbf{n}\, ds. \tag{44}$$

Inner products of (31) with $\psi_{x,y}$ determine the translation dynamics. Integration with ψ_x gives

$$\begin{aligned} X_t \cdot \hat{\mathbf{x}} \int_D \psi_x \frac{\partial h_0}{\partial x} d\mathbf{x} &= \int_{\partial D} \psi_x h_0^q \nabla \Delta h_q \cdot \mathbf{n}\, ds - \int_{\partial D} h_0^q (\Delta h_q) \nabla \psi_x \cdot \mathbf{n} ds \\ &\quad - \int_{\partial D} x \nabla h_q \cdot \mathbf{n} ds + \int_{\partial D} h_q \cos\theta\, ds \\ &\equiv \int_{\partial D} \psi_x J_q \cdot \mathbf{n}\, ds + B_1 + B_2 + B_3. \end{aligned} \tag{45}$$

In writing this, the inner products with $\partial h_0/\partial y$ and $\partial h_0/\partial R$ are zero by symmetry. We will argue that $B_1 = B_2 = B_3 = 0$.

First, since the leading order flux is constant across region II,

$$J_q \cdot \mathbf{n} = h_0^q \nabla \Delta h_q \cdot \mathbf{n} = \mathcal{O}(1), \quad r \to R. \tag{46}$$

Therefore

$$\nabla \Delta h_q \cdot \mathbf{n} = \mathcal{O}(|r-R|)^{-q}, \quad \Delta h_q = \mathcal{O}(|r-R|^{-q+1}), \quad r \to R. \tag{47}$$

Using (40) this means that

$$h_0^q (\psi_x)_z \Delta h_q = \mathcal{O}(|r-R|^{-q+2}), \quad r \to R \tag{48}$$

so that integral $B_1 = 0$.

For the integrals B_2 and B_3, consider first the sub-case $q = 1$. The relevant matching conditions are

$$h_1(R,\theta) = \lim_{z\to\infty} H_1(z), \quad (h_1)_r(R,\theta) = \lim_{z\to\infty} H_2'(z). \tag{49}$$

Since H_1 and H_2 are independent of θ, the integrals B_2 and B_3 vanish by symmetry.

For noninteger q, the terms in the region II expansion necessary for matching would be orders ϵ^q and ϵ^{q+1}. If such orders were included in the expansion, they would solve equations like

$$\Big(H_1^q [(H_n)_{zz} - U''(H_1) H_n]_z \Big)_z = 0. \tag{50}$$

where $1 < n < 3$. Since there is no flux of order $\epsilon^{q+n-3} > \epsilon^q$, integrating (50) one gets

$$(H_n)_{zz} - U''(H_1) H_n = \text{constant}. \tag{51}$$

From this it is seen that the solution H_n of *any* order $n < 3$ is independent of θ, and therefore the integrals B_2 and B_3 again vanish.

We now return to determining the migration dynamics. A similar argument as presented holds for for the inner product with ψ_y. Using (41,45) and $\mathbf{n} = (\cos\theta, \sin\theta)$ leads to

$$X_t = -\frac{1}{\pi}\frac{R\Psi(R)}{\int_0^R \Psi(r) r^2 dr}\left(\int_{\partial D} \mathbf{n} J_q \cdot \mathbf{n}\, ds\right). \tag{52}$$

Equations (43), (52) specify the droplet dynamics once the boundary value problem (27) - (29) is solved.

4.2 Case $q \in (2,3)$

As for the case of $p \leq 2$, in region II the flux of order ϵ^q involves the correction to H of order ϵ^3, which satisfies the linear equation

$$0 = (J_q \cdot \hat{\mathbf{z}})_z = \left(H_1^q[(H_3)_{zz} - R^{-1}(H_2)_z - zR^{-2}(H_1)_z + \frac{1}{2}U'''(H_1)H_2^2 + U''(H_1)H_3]_z\right)_z. \tag{53}$$

The relevant solvability condition for the linear equation (53) is found by using the bounded function

$$\Phi(z) = -\int_z^\infty \frac{H_1 - 1}{H_1^q} dz' \tag{54}$$

which is in the adjoint nullspace of the linear operator in (53) and corresponds to translation. Taking an inner product with (53) gives

$$\begin{aligned} 0 = &\Big[(J_q \cdot \hat{\mathbf{z}})\,\Phi - (H_1 - 1)[(H_3)_{zz} - U''(H_1)H_3] + (H_1)_z(H_3)_z - (H_1)_{zz}(H_3)\Big]_{-\infty}^{\infty} \\ &+ Q, \quad Q = \int_{-\infty}^{\infty} (H_1 - 1)[R^{-1}(H_2)_z + zR^{-2}(H_1)_z + \frac{1}{2}U'''(H_1)H_2^2]_z dz. \end{aligned} \tag{55}$$

Here $(J_q \cdot \hat{\mathbf{z}}) = -(J_q \cdot \mathbf{n})$ is just the flux matched to the region III solution at $z = -\infty$. Note that the term Q inherits radial symmetry from H_1, H_2 and therefore should be inconsequential for migration dynamics.

Applying the far field and matching conditions

$$\Phi \sim 0,\ (H_1)_z \sim 1,\ (H_3)_z \sim +\frac{\partial^2 h_1}{\partial r^2}(R,\theta)z - \frac{\partial h_2}{\partial r}(R,\theta), \qquad z \to \infty \tag{56}$$

$$H_1 \sim 1, \qquad z \to -\infty \tag{57}$$

to (55) gives

$$\left(J_q \cdot \hat{\mathbf{z}}\right) \int_{-\infty}^{\infty} \frac{H_1 - 1}{H_1^q} dz' = \frac{\partial h_2}{\partial r}(R,\theta) - Q. \tag{58}$$

In region I, we expand $h = h_0(x,t) + \epsilon h_1 + \epsilon^2 h_2 + o(\epsilon^2)$, and obtain the same as (31), except that it applies to the correction at order ϵ^2 instead of order ϵ^q:

$$\mathcal{L}h_2 = X_t \cdot \nabla h_0 - R_t \frac{\partial h_0}{\partial R}, \quad \mathcal{L} = (\nabla \cdot [h_0^q \nabla)\Delta, \quad \mathbf{x} \in D. \tag{59}$$

Solvability conditions are obtained as in case $q < 2$. An inner product with ψ_R gives

$$R_t = -\frac{\int_{\partial D} h_0^q \nabla \Delta h_2 \cdot \mathbf{n}\, ds}{\int_D \partial h_0 / \partial R \, dx}. \tag{60}$$

Note that $h_0^q \nabla \Delta h_2$ would be the flux at order ϵ^2, but this is zero since the leading order flux scales like ϵ^q. This means is $R_t = 0$ on the timescale specified by $\tau(\epsilon)$. One could potentially obtain the slow dynamics for mass exchange by going further in the expansion, where a result like (43) should follow on a timescale ϵ^q instead of $\tau(\epsilon)$.

For exponents $q \geq 2$ the functions ψ_x, ψ_y are not bounded at $r = R$, but we can integrate over a smaller disk D_ρ of radius ρ and take $\rho \to R$. To avoid excessive notation, the integrals $\int_D$, $\int_{\partial D}$ which appear below should be interpreted as this limit. Integration with ψ_x yields

$$\begin{aligned} X_t \cdot \hat{\mathbf{x}} \int_D \psi_x (h_0)_x \, d\mathbf{x} &= \int_{\partial D} \psi_x h_0^q \nabla \Delta h_2 \cdot \mathbf{n} ds - \int_{\partial D} h_0^q (\Delta h_2) \nabla \psi_x \cdot \mathbf{n} ds \\ &\quad - \int_{\partial D} x \nabla h_2 \cdot \mathbf{n} ds + \int_{\partial D} h_2 \cos\theta \, ds \\ &\equiv B_1 + B_2 + B_3 + B_4. \end{aligned} \tag{61}$$

In contrast to $p < 2$, only the boundary term B_3 is not zero. In light of (39), one has the asymptotics

$$\psi_x = \mathcal{O}(|r-R|^{2-q}), \quad \nabla \psi_x \cdot \mathbf{n} = \mathcal{O}(|r-R|^{1-q}), \quad h_0^q = \mathcal{O}(|r-R|^q). \tag{62}$$

The boundedness of derivatives of h_2 then imply $B_1 = B_2 = 0$. For B_4, matching to region I implies $H_2 \sim \frac{1}{2}(h_0)_{rr}(R,\theta) z^2 - (h_1)_r(R,\theta) z + (h_2)(R,\theta)$

for large z. This means that h_2 is independent of θ and symmetry gives $B_4 = 0$. It follows that

$$X_t \cdot \hat{\mathbf{x}} \int_D \psi_x (h_0)_x \, d\mathbf{x} = -\int_{\partial D} x \nabla h_2 \cdot \mathbf{n} ds \tag{63}$$

A similar expression can be obtained using ϕ_y. Combining with (58), the terms involving Q drop away by symmetry, leaving

$$X_t = -\frac{1}{\pi} \frac{R^2 \int_{-\infty}^{\infty} H_1^{1-q} - H_1^{-q} dz'}{\int_0^R \Psi(r) r^2 dr} \left(\int_{\partial D} \mathbf{n} J_q \cdot \mathbf{n} ds \right) \tag{64}$$

4.3 Case $q > 3$

The expansion in region II is now done as $H = \epsilon H_1 + \epsilon^2 H_2 + \epsilon^3 H^3 + \ldots$. At the level of the fist nonzero flux J_q, we get the linear equation

$$-(X_t \cdot \mathbf{n})(H_1)_z = \left(H_1^q [(H_3)_{zz} - R^{-1}(H_2)_z - zR^{-2}(H_1)_z + \frac{1}{2} U'''(H_1) H_2^2 + U''(H_1) H_3]_z \right)_z. \tag{65}$$

The solvability argument proceeds as for the case $2 < q < 3$, and uses the bounded function Φ defined in (54). The inner product with (65) gives the same result as for $2 < q < 3$ except that the left hand side is nonzero:

$$(X_t \cdot \mathbf{n}) \int_{-\infty}^{\infty} \frac{H_1 - 1}{H_1^{q-1}} dz = -(J_q \cdot \mathbf{n}) \int_{-\infty}^{\infty} \frac{H_1 - 1}{H_1^q} dz - \frac{\partial h_2}{\partial r}(R, \theta) - Q. \tag{66}$$

Here $(J_q \cdot \mathbf{n}) = -(J_q \cdot \hat{\mathbf{z}})(z = -\infty)$ is the flux matched to region III.

The expansion in region I is $h = h_0 + \epsilon h_1 + \epsilon^2 h_2 + o(\epsilon^2)$ which means h_2 solves

$$\nabla \cdot (h_0^q \nabla \Delta h_2) = 0. \tag{67}$$

This is the homogeneous version of (59), and therefore the relevant solvability conditions (for each coordinate direction) are the same as (63) with the left hand side suppressed:

$$\int_{\partial D} x \nabla h_2 \cdot \mathbf{n} ds = 0 = \int_{\partial D} y \nabla h_2 \cdot \mathbf{n} ds. \tag{68}$$

We can now multiply (66) by x or y and integrate over ∂D and use (68). Again the Q term drops away and we are left with

$$X_t = -\frac{1}{\pi} \frac{\int_{-\infty}^{\infty} H_1^{1-q} - H_1^{-q} dz'}{R \int_{-\infty}^{\infty} H_1^{2-q} - H_1^{1-q} dz'} \left(\int_{\partial D} \mathbf{n} J_q \cdot \mathbf{n} ds \right). \tag{69}$$

4.4 Case $q = 2$

This case is similar to $q \in (2,3)$, but there are logarithmically diverging terms that require care. The flux of order ϵ^2 in region II satisfies the linear equation

$$0 = (J_2 \cdot \hat{\mathbf{z}})_z = \left(H_1^2[(H_3)_{zz} - R^{-1}(H_2)_z - zR^{-2}(H_1)_z + \frac{1}{2}U'''(H_1)H_2^2 + U''(H_1)H_3]_z \right)_z. \tag{70}$$

which again says that the normal component of the flux is constant. The relevant solvability condition uses the function

$$\Phi = \int_{-\infty}^{z} \frac{H_1 - 1}{H_1^2} dz'. \tag{71}$$

which diverges logarithmically:

$$\Phi = \ln(z) + O(1), \quad z \to \infty. \tag{72}$$

Multiplying Φ by (70) and integrating from $-\infty$ to Z (since the result is unbounded as $Z \to \infty$) gives a result similar to (55)

$$\begin{aligned} 0 = &\Big[(J_2 \cdot \hat{\mathbf{z}})\, \Phi - (H_1 - 1)[(H_3)_{zz} - U''(H_1)H_3] + (H_1)_z(H_3)_z - (H_1)_{zz}(H_3) \Big]_{-\infty}^{Z} \\ &+ Q, \quad Q = \int_{-\infty}^{Z} (H_1 - 1)[R^{-1}(H_2)_z + zR^{-2}(H_1)_z + \frac{1}{2}U'''(H_1)H_2^2]_z dz. \end{aligned} \tag{73}$$

Since the flux J_2 is nonzero, integrating (70) directly gives $(H_3)_{zzz} \sim 1/z^2$ for large z. Therefore H_3 is bounded and $(H_3)_z$ diverges logarithmically as $z \to +\infty$. The balance of logarithmically diverging terms in (73) gives

$$(H_3)_z = (J_2 \cdot \mathbf{n}) \ln(z) + O(1), \quad z \to \infty, \tag{74}$$

where $(J_q \cdot \mathbf{n}) = -(J_q \cdot \hat{\mathbf{z}})(z = -\infty)$ is the flux matched to region III.

In region I, we expand $h = h_0(x,t) + \epsilon h_1 + \epsilon^2 \ln(1/\epsilon) h_* + o(\epsilon^2 \ln(1/\epsilon))$. Then h_* solves the linear equation (31), and the solvability arguments proceed as before. Like the case $q \in (2,3)$, $R_t = 0$ to leading order (albeit mass exchange is only logarithmically slower). The other solvability conditions are obtained by taking inner products with ψ_x, ψ_y, which produces a result analogous to (63):

$$X_t \cdot \hat{\mathbf{x}} \int_D \psi_x (h_0)_x \, d\mathbf{x} = -\int_{\partial D} x \nabla h_* \cdot \mathbf{n} ds. \tag{75}$$

Matching conditions that relate $(h_*)_x$ to $(H_3)_z$ are now derived. It is assumed that region I and II solutions describe the same solution on some overlapping region $1 \ll z \ll [\epsilon \ln(1/\epsilon)]^{-1}$. Within this region, a Taylor expansion is justified for h_0, h_1 but not h_* so that

$$\begin{aligned}
&(H_1)_z + \epsilon(H_2)_z + \epsilon^2(H_3)_z + o(\epsilon^2) \\
&= -(h_0)_r - \epsilon(h_1)_r - \epsilon^2 \ln(1/\epsilon)(h_*)_r + o(\epsilon^2 \ln(1/\epsilon)) \\
&= -(h_0)_r(R,\theta) - \epsilon\Big[(h_1)_r(R,\theta) + (h_0)_{rr}(R,\theta)z\Big] - \epsilon^2 \ln(1/\epsilon)(h_*)_r(R,\theta) + o(\epsilon^2 \ln(1/\epsilon)).
\end{aligned} \tag{76}$$

Equating terms at order 1 and ϵ gives the usual matching conditions for regular expansions. For the logarithmic terms, the procedure is to take $\epsilon \to 0$ and $z \sim [\epsilon \ln(1/\epsilon)]^{-1}$ simultaneously. Using (74), for large z have

$$(H_3)_z = (J_2 \cdot \mathbf{n}) \ln\Big([\epsilon \ln(1/\epsilon)]^{-1}\Big) + O(1) = (J_2 \cdot \mathbf{n}) \ln(1/\epsilon) + \mathcal{O}\Big(\ln(\ln(1/\epsilon))\Big). \tag{77}$$

Inserting into (76) and equating terms of order $\epsilon^2 \ln(1/\epsilon)$ gives

$$(J_2 \cdot \mathbf{n}) = -(h_*)_r(R,\theta). \tag{78}$$

This can be combined with (75) to yield

$$X_t = -\frac{1}{\pi} \frac{R^2}{\int_0^R \Psi(r) r^2 dr} \left(\int_{\partial D} \mathbf{n} J_q \cdot \mathbf{n} \, ds \right). \tag{79}$$

4.5 Case $q = 3$

This case is similar to both $q > 3$ and $q \in (2,3)$, but there are again logarithmically diverging terms. The flux of order ϵ^3 in region II satisfies the linear equation

$$0 = (J_3 \cdot \hat{\mathbf{z}})_z = \Big(H_1^3[(H_3)_{zz} - R^{-1}(H_2)_z - zR^{-2}(H_1)_z + \frac{1}{2}U'''(H_1)H_2^2 + U''(H_1)H_3]_z \Big)_z. \tag{80}$$

A solvability argument identical to the case $q \in (2,3)$ produces

$$(J_3 \cdot \mathbf{n}) \int_{-\infty}^{\infty} \frac{H_1 - 1}{H_1^3} dz' = (H_3)_z - Q. \tag{81}$$

In region I, we expand $h = h_0(x,t) + \epsilon h_1 + \epsilon^2/\ln(1/\epsilon) h_* + o(\epsilon^2/\ln(1/\epsilon))$, so that h_* solves the linear equation (31) with $q = 3$, and the solvability

arguments proceed as before. As for all cases $q \geq 2$, $R_t = 0$ to leading order. In this case, the inner products with ψ_x, ψ_y diverge logarithmically, so we integrate on a disk $D(\rho)$ with radius $\rho < R$ and consider the asymptotics as $\rho \to R$. Multiplying by ψ_x and integrating gives

$$(X_t \cdot \hat{\mathbf{x}}) \int_{D(\rho)} \psi_x (h_0)_x \, d\mathbf{x} = \int_{\partial D(\rho)} \psi_x h_0^3 \nabla \Delta h_* \cdot \mathbf{n} ds - \int_{\partial D(\rho)} h_0^3 (\Delta h_*) \nabla \psi_x \cdot \mathbf{n} ds$$
$$- \int_{\partial D(\rho)} x \nabla h_* \cdot \mathbf{n} ds + \int_{\partial D(\rho)} h_* \cos\theta \, ds = B_1 + B_2 + B_3 + B_4. \tag{82}$$

The integral on the left hand side has a logarithmic singularity as $\rho \to R$ because of (39), in particular

$$\int_{D(\rho)} \psi_x (h_0)_x \, d\mathbf{x} = -\pi R^2 \ln|R - \rho| + \mathcal{O}(1), \quad \rho \to R. \tag{83}$$

Matching conditions (which are detailed below) require $\nabla h_* \sim C \ln|R - r|$. As a consequence, we find that h_* is bounded and

$$\nabla \Delta h_* \sim |R - r|^{-2}, \quad \Delta h_* \sim |R - r|^{-1} \tag{84}$$

as $r \to R$. All this implies that the integrals B_1, B_2, B_4 are bounded as $\rho \to R$ but B_3 diverges logarithmically. Using (82-83) gives

$$\int_{\partial D(\rho)} x \nabla h_* \cdot \mathbf{n} ds = \pi R^2 (X_t \cdot \hat{\mathbf{x}}) \ln|R - \rho| + \mathcal{O}(1), \quad \rho \to R. \tag{85}$$

The matching condition that relates $(h_*)_r$ to $(H_3)_z$ is derived as for $q = 2$. Equating expansions for h_r in regions I and II, then for $1 \ll z \ll \log(1/\epsilon)$,

$$\begin{aligned}
&(H_1)_z + \epsilon (H_2)_z + \epsilon^2 (H_3)_z + o(\epsilon^2) \\
&= -(h_0)_r - \epsilon (h_1)_r - \epsilon^2 / \ln(1/\epsilon) (h_*)_r + o(\epsilon^2 / \ln(1/\epsilon)) \\
&= -(h_0)_r(R, \theta) - \epsilon \Big[(h_1)_r(R, \theta) + (h_0)_{rr}(R, \theta) z \Big] \\
&- \epsilon^2 (h_1)_{rr}(R, \theta) z - \epsilon^2 / \ln(1/\epsilon) (h_*)_r + o(\epsilon^2 / \ln(1/\epsilon))
\end{aligned} \tag{86}$$

Let $(h_*)_r \sim C \ln|R - r|, r \to R$ where C is to be determined. Taking $\epsilon \to 0$ with $z \sim \ln(1/\epsilon)$ simultaneously implies for large z

$$(h_*)_r = C \ln(\epsilon z) + \mathcal{O}(1) = C \ln(\epsilon) + \mathcal{O}(\ln(\ln(1/\epsilon))), \quad \epsilon \to 0. \tag{87}$$

Inserting into (86) and equating terms of order ϵ^2 we obtain

$$C = \lim_{z\to\infty} -(H_3)_z. \tag{88}$$

Finally, combining (81), (85), (88),

$$X_t = -\frac{1}{\pi}\frac{\int_{-\infty}^{\infty} H_1^{-2} - H_1^{-3} dz}{R}\left(\int_{\partial D} \mathbf{n} J_q \cdot \mathbf{n}\, ds\right). \tag{89}$$

5 Effective medium approximation and identification of timescales

One potentially useful approximation to the free boundary problem described in section 2 utilizes Green's functions similar to the effective medium approximations for standard Ostwald ripening [20]. This is employed to determine timescales for a large system of interacting droplets.

5.1 Reduced system

Let X_k, R_k, $k = 1, \ldots, N$ be the droplet centers and radii. We want to solve $\Delta P = 0$ exterior to the droplets, i.e. for all $\mathbf{x}, |\mathbf{x} - X_k| > R_k$, subject to the boundary conditions

$$P(\mathbf{x}) = \frac{2}{R_k}, \quad |\mathbf{x} - X_k| = R_k. \tag{90}$$

The simplest approximation looks for a solution as a sum of Green's functions

$$P(\mathbf{x}) = B_0 + \sum_{k=1}^{N} B_k \ln|\mathbf{x} - X_k|^2. \tag{91}$$

For each $j = 1 \ldots N$, the boundary condition which one wishes to satisfy is

$$\frac{2}{R_j} = B_0 + \sum_{k=1}^{N} B_k \ln|\mathbf{x} - X_k|^2, \quad \text{for } \ |\mathbf{x} - X_j| = R_j. \tag{92}$$

Assuming the droplets are well separated, the approximation $|\mathbf{x} - X_k| \approx |X_j - X_k|$ holds on the boundary of droplet $j \neq k$, giving

$$\frac{2}{R_j} = B_0 + B_j \ln(R_j^2) + \sum_{k\neq j} B_k \ln|X_j - X_k|^2, \quad j = 1, \ldots, N. \tag{93}$$

The system is completed by the requirement that there is no flux at infinity:

$$\int_S \nabla P \cdot n \to 0, \tag{94}$$

as the curve S (take it to be a giant circle) is taken out to infinity. As $\mathbf{x} \to \infty$, $1/|\mathbf{x} - R_k| \approx 1/|\mathbf{x}|$ and therefore

$$\int_S \nabla P \cdot n \to \sum_{k=1}^{N} B_k \left(\int_S \frac{1}{|\mathbf{x}|} ds \right) = 2\pi \sum_{k=1}^{N} B_k. \tag{95}$$

This integral will be zero only if

$$\sum_{k=1}^{N} B_k = 0. \tag{96}$$

Equations (93) and (96) define a $(N+1) \times (N+1)$ linear problem to be solved.

The integral in (9) to be computed for each j is

$$\int_{\partial D_j} J \cdot \mathbf{n}\, ds = -\int_{\partial D_j} \nabla P \cdot \mathbf{n}\, ds = 4\pi B_j. \tag{97}$$

The integral in (10) to be evaluated for each j is

$$\begin{aligned} \int_{\partial D_j} (J \cdot \mathbf{n})\mathbf{n}\, ds &= -\int_{\partial D_j} \left(\sum_k B_k \frac{2(\mathbf{x} - X_k) \cdot \mathbf{n}}{|\mathbf{x} - X_k|^2} \right) ds(\mathbf{x}) \\ &\approx -2 \left(\sum_{k \neq j} B_k \frac{X_j - X_k}{|X_j - X_k|^2} \right) \cdot \left(\int_{\partial D_j} \mathbf{n} \otimes \mathbf{n}\, ds \right) \end{aligned} \tag{98}$$

where the same approximation $|\mathbf{x} - X_k| \approx |X_j - X_k|$ as before was used. Since

$$\int_{\partial D_j} \mathbf{n} \otimes \mathbf{n}\, ds = \pi R_j \mathbf{I}, \tag{99}$$

where $\mathbf{I}$ is the identity matrix, it follows

$$\int_{\partial D_j} (J \cdot \mathbf{n})\mathbf{n}\, ds \approx -2\pi R_j \sum_{k \neq j} B_k \frac{X_j - X_k}{|X_j - X_k|^2}. \tag{100}$$

5.2 Dynamic timescales

Consider now a reasonably large array of droplets which all have a similar size R and typical spacing L, so that the volume per unit area is

$$H_{average} = \frac{R^3}{L^2} \tag{101}$$

which is constant as time progresses.

Timescale for ripening. The approximation (91) gives the scaling

$$B_j \sim R^{-1}/\ln L \tag{102}$$

which with (97) further implies

$$\int_{\partial D_j} J \cdot \mathbf{n}\, ds \sim R^{-1}/\ln L. \tag{103}$$

For exponents $q < 2$, using (9), the timescale for ripening (i.e. mass exchange) can be computed as

$$\tau_{ripe} \sim \frac{R}{R_t} \sim R^4 \ln L \sim H_{average}^{4/3} L^{8/3} \ln L, \quad q < 2. \tag{104}$$

For exponents $q \geq 2$, the ripening dynamics occur on a timescale of the flux, i.e. ϵ^q, rather than $\tau(\epsilon)$. This can be accommodated by including an extra factor in the timescale:

$$\tau_{ripe} \sim \frac{R}{R_t} \sim \frac{\tau(\epsilon)}{\epsilon^q} H_{average}^{4/3} L^{8/3} \ln L, \quad q \geq 2. \tag{105}$$

Timescale for migration. Using (100) and (102) one can obtain

$$\int_{\partial D_j} (J \cdot \mathbf{n})\mathbf{n}\, ds \sim L^{-1}/\ln L. \tag{106}$$

Using (10), the timescale for migration can be computed as

$$\tau_{mig} \sim \frac{L}{X_t} \sim \begin{cases} H_{average}^{2/3} L^{10/3} \ln L & q < 2 \\ H_{average}^{\frac{4-q}{3}} L^{(14-2q)/3} \ln L & q \in [2,3] \\ H_{average}^{1/3} L^{8/3} \ln L & q > 3 \end{cases} \tag{107}$$

The limit of large droplet size in the unscaled equation. Here we show that our scaling results are, suitably interpreted, the same as those derived in the companion paper [4]. The starting point there was the unscaled thin film equation

$$h_t = \nabla \cdot (h^q \nabla p), \quad p = U'(h) - \Delta h, \quad q > 0. \tag{108}$$

In [4], the limit of large droplet volume was considered, in contrast to small precursor film. In this case, let $V \gg 1$ be a typical droplet volume with characteristic inter-droplet distance L'. This suggests the natural small parameter is $\epsilon = V^{-1/3}$. Rescaling (108) using

$$x \to \epsilon^{-1} x, \quad t \to \tau(\epsilon)^{-1} \epsilon^{q-4}, \quad h \to h\epsilon^{-1} \tag{109}$$

gives exactly (1). The average droplet size after rescaling is $R = 1$, and the characteristic distance between droplets is

$$L = \epsilon L' = \frac{V^{1/6}}{\overline{H}^{1/2}} \tag{110}$$

where $\overline{H} = V/(L')^2$. The mass density for the scaled equation is

$$H_{average} = \frac{1}{\epsilon^2 (L')^2} = \frac{\overline{H}}{V^{1/3}} \tag{111}$$

Timescales with respect to the unscaled equation (108) can now be written in terms of V and $\overline{H}$. For the ripening times given by either (104),(105) one obtains

$$\tau_{ripe}^{unscaled} = \tau(\epsilon)\epsilon^{4-q}\tau_{ripe} \sim V^{4/3} \ln V + \mathcal{O}(1), \quad V \to \infty. \tag{112}$$

For the migration timescale (107) one has

$$\tau_{mig}^{unscaled} = \tau(\epsilon)\epsilon^{4-q}\tau_{mig} = \mathcal{O}(1) + \frac{1}{\overline{H}} \begin{cases} V^{5/3} \ln V & q \in (0,2) \\ V^{5/3} & q = 2 \\ V^{\frac{7-q}{3}} \ln V & q \in (2,3) \\ V^{4/3} \ln^2 V & q = 3 \\ V^{4/3} \ln V & q > 3 \end{cases}, \quad V \to \infty. \tag{113}$$

6 Computational examples

We conclude by using the approximations of the previous section to study the evolution of a large assembly of droplets. We focus on the most relevant mobility exponent $q = 3$, which corresponds to a fluid with Newtonian viscosity and a no-slip boundary condition. In doing this, the exchange of material between droplets is ignored, and only the leading-order effect, migration, is considered. There are no boundaries in the calculation, so that

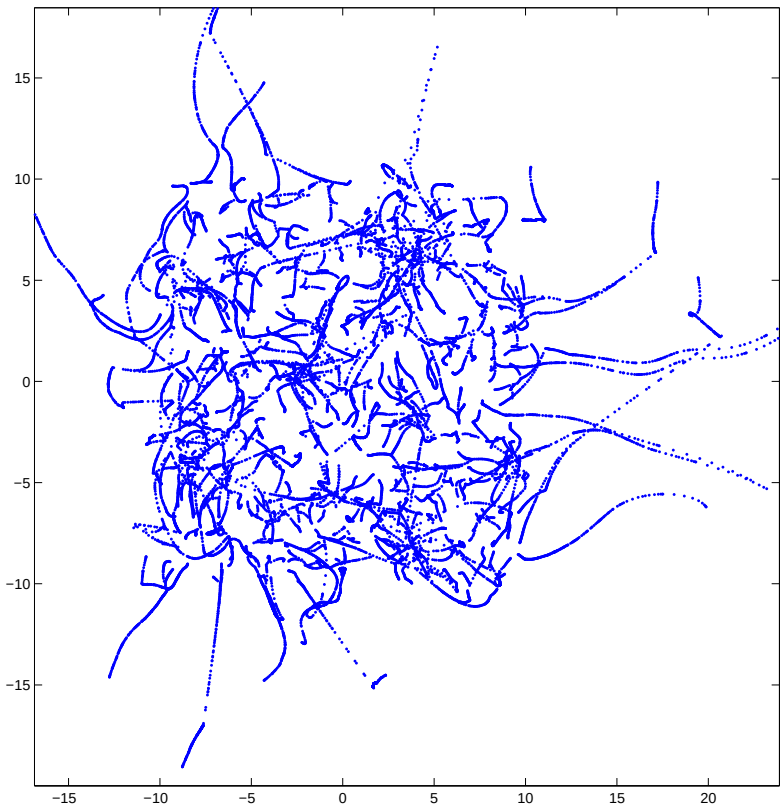

Figure 2: Trajectories for a simulation with 500 initial droplets ($q = 3$). Note that small, un-coalesced droplets on the fringes are repelled.

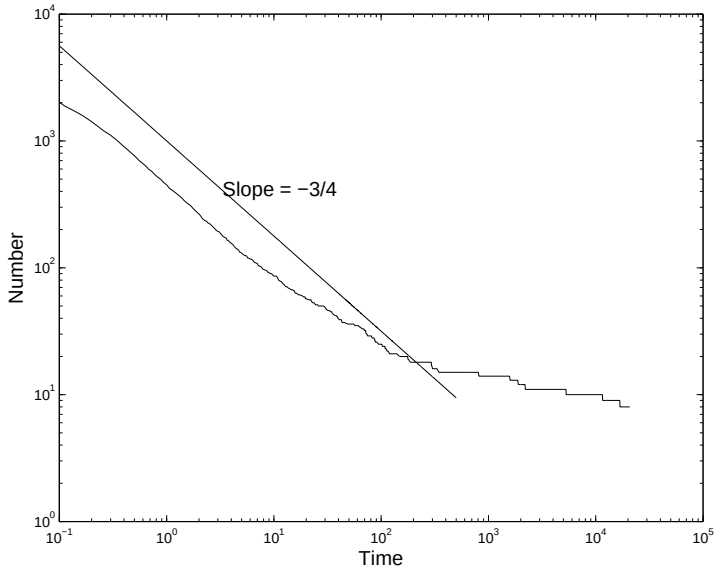

Figure 3: Dynamic scaling of coalescence-driven coarsening (q=3), using 5000 initial droplets. A line with slope $-3/4$ is provided for comparison to the predictions of [14].

(94) applies. An ad-hoc criteria for coalescence is applied, which states that when the perimeters of two droplets overlap, their volume is combined and the center of mass is preserved.

Figure 2 is an illustration of the dynamics. The simulation was started with 500 droplets in random locations, each with a random but nearly uniform radius. Droplets in the middle of the assembly coalesce first, simply because they have a greater number of neighbors. As time progresses, it follows that smaller, more mobile droplets on the fringes will be driven away, since the motion is opposite the flux, which is toward larger droplets. The amount of time droplets take to move (relative to the inter-droplet distance) increases since the driving force given by flux decreases with increasing droplet size.

Figure 3 shows the droplet number plotted as a function of time, for a simulation with 5000 droplets initially. Dynamic scaling of the coarsening process was predicted [14]; in particular the relevant length scale (the typical inter-droplet distance L) should increase as $t^{3/8}$. Since the number of

droplets N scales according to

$$NL^2 \sim \text{area of domain}$$

then N should scale in time like $t^{-3/4}$. This is more or less born out by the results in figure 3. At late times when the array has spread out to a somewhat larger area, there is a slowing of the coarsening process, also seen in the computational results.

Acknowledgments

The author is grateful for discussions with Felix Otto, Tobias Rump and Dejan Slepcev, and for the hospitality afforded during his visit to the University of Bonn. This work was produced with assistance of NSF award DMS-0405596.

References

[1] J. Becker, G. Grun, R. Seemann, H. Mantz, K. Jacobs, K. R. Mecke, and R. Blossey, *Complex dewetting scenarios captured by thin-film models*, Nature Materials, 2 (2003), pp. 59–53.

[2] A. L. Bertozzi, G. Grun, and T. P. Witelski, *Dewetting films: bifurcations and concentrations*, Nonlinearity, 14 (2001), pp. 1569–1592.

[3] J. W. Cahn and J. E. Hilliard, *Free energy of a nonuniform system I: Interfacial free energy*, J. Chem. Phys., 28 (1957), pp. 258–267.

[4] K. Glasner, F. Otto, T. Rump, and D. Slepcev, *Ostwald ripening of droplets: The role of migration*, preprint, (2007).

[5] K. B. Glasner and T. P. Witelski, *Coarsening dynamics of dewetting films*, Phys. Rev. E, 67 (2003), p. 016302.

[6] K. B. Glasner and T. P. Witelski, *Collision versus collapse of droplets in coarsening of dewetting thin films*, Phys. D, 209 (2005), pp. 80–104.

[7] I. M. Lifshitz and V. V. Slyozov, *The kinetics of precipitation from supersaturated solid solutions*, J. Chem. Phys. Solids, 19 (1961), pp. 35–50.

[8] R. Limary and P. F. Green, *Late-stage coarsening of an unstable structured liquid film*, Phys. Rev. E, 66 (2002).

[9] ——, *Dynamics of droplets on the surface of a structured fluid film: Late-stage coarsening*, Langmuir, 19 (2003), pp. 2419–2424.

[10] V. Mitlin and N. V. Petviashvilli, *Nonlinear dynamics of dewetting: kinetically stable structures*, Phys. Lett. A, 192 (1994), p. 323.

[11] B. Niethammer and F. Otto, *Domain coarsening in thin films*, Comm. Pure Appl. Math., 54 (2001), pp. 361–384.

[12] B. Niethammer and R. L. Pego, *On the initial-value problem in the Lifshitz-Slyozov-Wagner theory of Ostwald ripening*, SIAM J. Math. Anal., 31 (2000), pp. 467–485 (electronic).

[13] L. Onsager, Physical Review, 38 (1931), p. 2265.

[14] F. Otto, T. Rump, and D. Slepčev, *Coarsening rates for a droplet model: rigorous upper bounds*, SIAM J. Math. Anal., 38 (2006), pp. 503–529 (electronic).

[15] R. L. Pego, *Front migration in the nonlinear Cahn-Hilliard equation*, Proc. R. Soc. Lond. A, 422 (1989), pp. 261–278.

[16] L. M. Pismen and Y. Pomeau, *Mobility and interactions of weakly nonwetting droplets*, Phys. Fluids, 16 (2004), pp. 2604–2612.

[17] G. Reiter, *Dewetting of thin polymer films*, Phys. Rev. Lett., 68 (1992), pp. 75–78.

[18] R. A. Segalman and P. F. Green, *Dynamics of rims and the onset of spinodal dewetting at liquid/ liquid interfaces*, Macromolecules, 32 (1999), pp. 801–807.

[19] A. Sharma and R. Khanna, *Pattern formation in unstable thin liquid films*, Phys. Rev. Let., 81 (1998), pp. 3463–3466.

[20] P. W. Voorhees, *The theory of Ostwald ripening*, J. Stat. Phys., 38 (1985), pp. 231–252.

[21] C. Wagner, *Theorie for alterung von niederschlagen durch umlosen*, Z. Elektrochemie, 65 (1961), pp. 581–594.

[22] R. Xie, A. Karim, J. F. Douglas, C. C. Han, and R. A. Weiss, *Spinodal dewetting of thin polymer films*, Phys. Rev. Let., 81 (1998), pp. 1251–1254.